Kinematic–dynamic modelling and numerical evaluation of joint torques for the Telemax EVO Plus manipulator*

Vitaliy Korendiy[1,*,†], Olga Duran[3,†], Pavlo Krot[2,†], Roman Karpyn[1,†] and Mykhailo Pylyp[1,†]

[1] *Lviv Polytechnic National University, 12, Stepan Bandera str., 79013, Lviv, Ukraine*

[2] *Wroclaw University of Science and Technology, Na Grobli 15, 50-421 Wroclaw, Poland*

[3] *Kingston University, Department of Mechanical Engineering, Faculty of Engineering, Computing and the Environment, Roehampton Vale, London SW15 3DW, United Kingdom*

Abstract

Unmanned ground vehicles equipped with manipulators are used for remote execution of high-risk tasks, including EOD and HAZMAT/CBRN applications. This paper develops a kinematic and dynamic modelling workflow for the Telemax EVO Plus 6-DoF serial manipulator and evaluates joint torque profiles under a prescribed stress trajectory. Forward kinematics are formulated using the Denavit–Hartenberg convention and extended with Jacobian-based expressions for link centre-of-mass velocities. Manipulator dynamics are derived using an energy-based Euler–Lagrange formulation; in the absence of experimental friction data, a viscous friction approximation is adopted. Joint torque profiles are evaluated numerically in Wolfram Mathematica by substituting prescribed joint trajectories.

The stress scenario is defined over 1 s with a smooth start/stop law (5th-order polynomial) and boundary values ϕ_0: 0°⟶180°, ϕ_1: 110°⟶55°, ϕ_2: −20°⟶0°, ϕ_3=ϕ_4=0°, and ϕ_5: 0°⟶360°. For this scenario, the peak torque magnitudes satisfy $|\tau_1|>|\tau_0|>|\tau_2|$, with representative peak levels $\tau_1 \approx -35\ldots-36$ Nm, $\tau_0 \approx +30\ldots31$ Nm during acceleration and $\tau_0 \approx -24\ldots-26$ Nm during braking, and $\tau_2 \approx -16\ldots-17$ Nm. Wrist torques are substantially smaller: τ_3 and τ_4 are reported as practically zero, while τ_5 reaches a maximum of approximately 0.34…0.36 Nm (about two orders of magnitude lower than τ_0–τ_2). Due to the lack of open-source inertial parameters for Telemax EVO Plus links, a consistent parameter set is adopted based on specification and geometric approximation, therefore, the reported torque levels should be interpreted as numerical estimates for the adopted parameter set and the specified scenario.

Keywords

Telemax EVO Plus, unmanned ground vehicle, serial manipulator

1. Introduction

Modern hybrid threats and local conflicts significantly increase the demand for remote execution of high-risk tasks. In particular, explosive ordnance disposal (EOD), chemical, biological, radiological and nuclear (CBRN/HAZMAT) operations, and reconnaissance in hazardous or inaccessible environments require reliable robotic platforms to ensure personnel safety. Consequently, unmanned ground vehicles (UGVs) equipped with manipulators have become a critical component of contemporary safety-oriented robotic systems.

However, the operation of robotic manipulators at the limits of their technical capabilities, especially at large horizontal reaches, is associated with critical dynamic loads. Gravitational forces, inertial moments during accelerated motion of massive links, and Coriolis effects may lead to platform tipping, actuator overheating, or mechanical failure of structural components. These risks significantly reduce reliability and underscore the need for accurate predictive modelling of manipulator dynamics.

* *SmartIndustry 2026: 3rd International Conference on Smart Automation & Robotics for Future Industry, March 26-27, 2026, Lviv, Ukraine*

[1*] Corresponding author.

[†] These authors contributed equally.

vitalii.m.korendii@lpnu.ua (V. Korendiy); O.Duran@kingston.ac.uk (O.Duran)

mykhailo.v.pylyp@lpnu.ua (M. Pylyp); roman.b.karpyn@lpnu.ua (R. Karpyn)

0000-0002-6025-3013 (V. Korendiy); 0000-0002-1397-6032 (O.Duran)

0009-0003-7964-0624 (M. Pylyp); 0009-0005-1695-492X (R. Karpyn)

Existing control algorithms are often limited to kinematic trajectory planning and do not fully account for transient dynamic effects. The absence of an adapted dynamic model for the specific configuration of the Telemax EVO Plus manipulator complicates the prediction of robot behaviour in stress operating regimes and limits the development of safety-oriented mission planning strategies. From a Smart Industry perspective, the developed kinematic and dynamic models constitute a physics-based digital representation of the Telemax EVO Plus manipulator, enabling predictive evaluation of actuator loads and stability constraints prior to mission execution. Such model-based simulation frameworks are essential components of cyber-physical robotic systems, supporting mission planning, safe operational envelope definition, and decision-making under high-risk conditions. In this context, the proposed modelling approach provides a computational foundation for digital twin–oriented analysis of mission-critical mobile manipulators.

2. Literature Review

Classical robotics literature establishes a theoretical foundation for manipulator modelling by combining kinematic and dynamic formulations. In this framework, manipulator dynamics are commonly described using Lagrangian and Newton–Euler approaches, with the equations of motion decomposed into inertia, velocity-dependent, and gravity components [1, 3, 9, 11, 14]. In the context of motion planning, the concept of kinodynamic motion planning was introduced to incorporate system dynamics into planning algorithms [2]. Building on these formulations, algorithmic approaches to rigid-body dynamics provide efficient computational methods for forward and inverse dynamics of articulated systems [4].

Complementary to this, a unified theoretical framework integrating mechanics, motion planning, and control for robotic systems is presented in [5]. Extending these concepts to systems with mobility, the problem of mobile manipulation, involving the coordinated operation of a mobile base and a manipulator, was formulated in [6].

From a modelling perspective, the kinematic representation of serial manipulators is commonly based on the Denavit–Hartenberg convention, which introduced a matrix-based notation for lower-pair mechanisms [7, 8]. Furthermore, computationally efficient schemes for manipulator dynamics, including recursive formulations and comparative analyses of dynamic modelling approaches, have been reported in the classical robotics literature [12, 13]. Finally, studies on workspace and manipulability analysis of robotic manipulators are reported in [13], while kinematic modelling of 6-DoF articulated robots with spherical wrists is presented in [14], further contributing to the methodological basis for analyzing serial manipulator configurations.

Within the domain of Explosive Ordnance Disposal (EOD) robotics, dedicated studies address the detection and identification of potentially explosive objects [15], while kinematic modelling of EOD robot manipulators has been reported in the literature [16]. In addition, prototype evaluation of EOD robotic platforms and control design approaches for EOD manipulators have been presented in [17]. Force control and impedance-based control strategies for bilateral teleoperated manipulation have also been investigated [18, 19], providing relevant methodological background for remote operation of robotic manipulators in hazardous environments.

For the specific robotic platform considered in this study, the specifications and structural parameters of the Telemax EVO Plus system are documented in manufacturer technical documentation [20, 21], which provide the necessary input data for the kinematic and dynamic modelling developed in this work.

This work investigates the Telemax EVO Plus robotic platform equipped with a variable-geometry tracked base and a 6-DoF manipulator. [20-22]. The Telemax EVO Plus platform is capable of manipulating payloads up to 80 kg [21, 22], which is associated with increased dynamic loads.

Existing control approaches are often focused on kinematic trajectory planning, while transient dynamic effects are not explicitly considered, which may affect mission reliability [1, 10].

Manipulator-induced dynamic loads can influence mobile manipulator stability and potentially cause platform tip-over [23], while actuator thermal limits may constrain operational performance and require thermal recovery strategies [24].

Although general manipulator dynamic models are available in the literature, platform-specific configurations require tailored modelling that accounts for geometry and system parameters. Accordingly, this work develops a comprehensive kinematic and force-based analysis to estimate joint torques and establish safe operating regimes.

Although generic kinematic and dynamic formulations for serial manipulators are well established, platform-specific modelling of EOD mobile manipulators with variable geometry and payload-dependent dynamics remains limited. In particular, existing studies rarely quantify actuator torque limits and stability constraints under stress trajectories and extended-reach manipulation scenarios. Furthermore, the interaction between telescopic link extension and joint load distribution is insufficiently addressed in the current literature. This gap motivates the development of a dedicated dynamic modelling and simulation framework for the Telemax EVO Plus manipulator.

The main contributions of this work are as follows:

- Development of a platform-specific dynamic model of the Telemax EVO Plus manipulator incorporating payload-dependent mass distribution and variable link geometry.
- Formulation of a simulation-based framework for evaluating joint torque limits under mission-relevant manipulation scenarios.
- Analysis of payload–reach constraints and stability-related operational envelopes for high-risk robotic manipulation tasks.

3. Methodology

The Telemax EVO Plus is a mobile robotic platform designed for remote manipulation tasks in hazardous environments, including EOD, HAZMAT, and CBRN operations.

3.1. System Description and Kinematics of the Telemax EVO Plus Manipulator

The Telemax EVO Plus is a tracked mobile robotic platform equipped with a serial manipulator intended for remote operation in hazardous environments such as EOD, HAZMAT, and chemical, biological, radiological, and nuclear (CBRN) scenarios. The system integrates a tracked mobile base with controllable flippers and a 6-DOF serial manipulator. Key technical specifications relevant to modelling are summarized in Table 1. The mobile platform consists of four independent tracked modules with electric drives and controllable flippers, which enhance terrain negotiation capabilities. The system is controlled via a ground control station with wireless communication. For the purposes of dynamic modelling, only the robotic platform and manipulator masses are considered, operator mass is excluded from the modelling framework.

Table 1
Technical Specifications of the Telemax EVO Plus Platform [20]

Parameter	Value	Unit
Overall dimensions (L × W × H)	870 × 680 × 740	mm
Platform weight without manipulator	113	kg
Maximum travel speed	5	km/h (3.1 mph)

Maximum manipulator payload	80	kg (176 lb)
Maximum vertical reach (with telescopic link)	2860	mm
Maximum horizontal reach	1860	mm
Gripper opening width	200	mm
Number of manipulator degrees of freedom	6	DOF
Continuous operation time	up to 12	h
Maximum slope climbing angle	45	degrees
Maximum obstacle height (with flippers)	400	mm
Maximum gap width	500	mm
Total system weight in operational configuration	~250	kg
Communication system	IP Mesh Radio Network	–
Chassis drive type	4-track drive with independent flippers	–

The manipulator is modelled as an open serial kinematic chain composed of six revolute joints. The degrees of freedom are distributed into three positioning and three orientation joints, enabling full control of the end-effector pose in Cartesian space. Although the platform includes a telescopic section, the telescopic extension is not explicitly modelled in the kinematic/dynamic formulation in this study, all link lengths are treated as constants in this study.

Manufacturer specifications indicate an inverse relationship between payload capacity and horizontal reach, which is used as a constraint in the modelling and simulation scenarios considered in this work. This relationship is summarized in Table 2. [20—22].

Table 2
Payload capacity versus horizontal reach of the Telemax EVO Plus manipulator

Payload capacity	Horizontal reach
80 kg	300 mm
45 kg	810 mm
25 kg	1180 mm
15 kg	1530 mm

The manipulator is modelled as a 6-axis serial chain comprising six revolute joints. Table 3 summarises a typical joint configuration used in EOD robotic manipulators, including the joint motion type and the corresponding angular ranges.

Table 3
Joint types and motion ranges

Joint	Type of movement	Range	Example of starting position
1	Revolute	±160°	Rotation at the base
2	Revolute	±90°	Raising/lowering the main link
3	Revolute	±90°	Raising/lowering the second link
4	Revolute	±180°	Rotation of the wrist (Roll)
5	Revolute	±90°	Tilt of the wrist (Pitch)
6	Revolute	±180°	Rotation of the end effector (Yaw)

The manipulator working zones and maximum operational reach are illustrated in Figure 1. These workspace limits define the geometric constraints for the simulation scenarios considered in this study.

Figure 1:

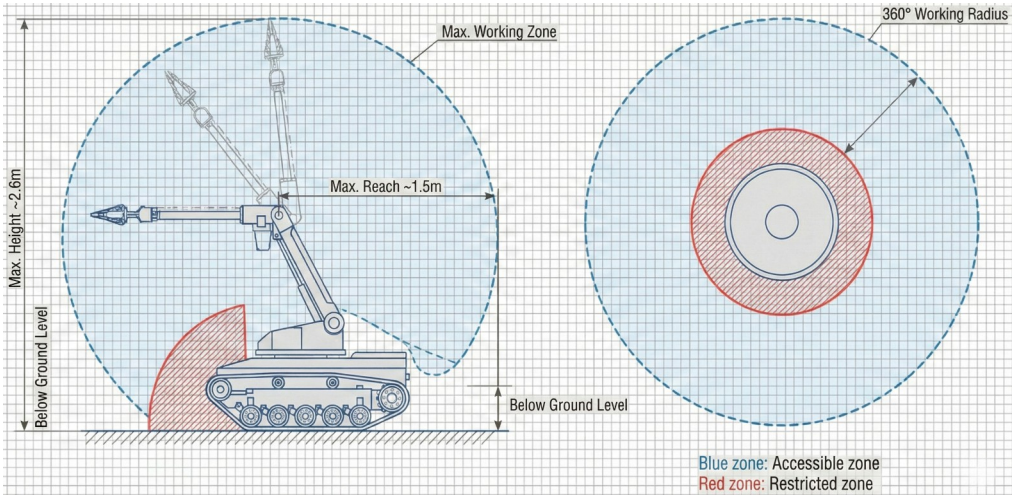

Manipulator working zones and maximum operating reach of the Telemax EVO Plus platform.

The Telemax EVO Plus manipulator is an open serial spatial mechanism as shown in the kinematic diagram (Figure 2) comprising six moving links connected by six one-DoF revolute joints (all joints are lower pairs of class 5). The fixed base link is the robot body, the subsequent links are connected sequentially (turret, shoulder, forearm/ intermediate sections, wrist, and end effector/gripper), with no closed kinematic loops, which enables a direct matrix-based kinematic description. Using the Somov–Malyshchev mobility formula for spatial mechanisms with $n=6$, $p_5=6$, $p_1=p_3=p_4=0$ the mobility is $W=6\cdot6-5\cdot6=6$, confirming six degrees of freedom that allow independent positioning and orientation of the end effector in 3D space with three translational and three rotational coordinates.

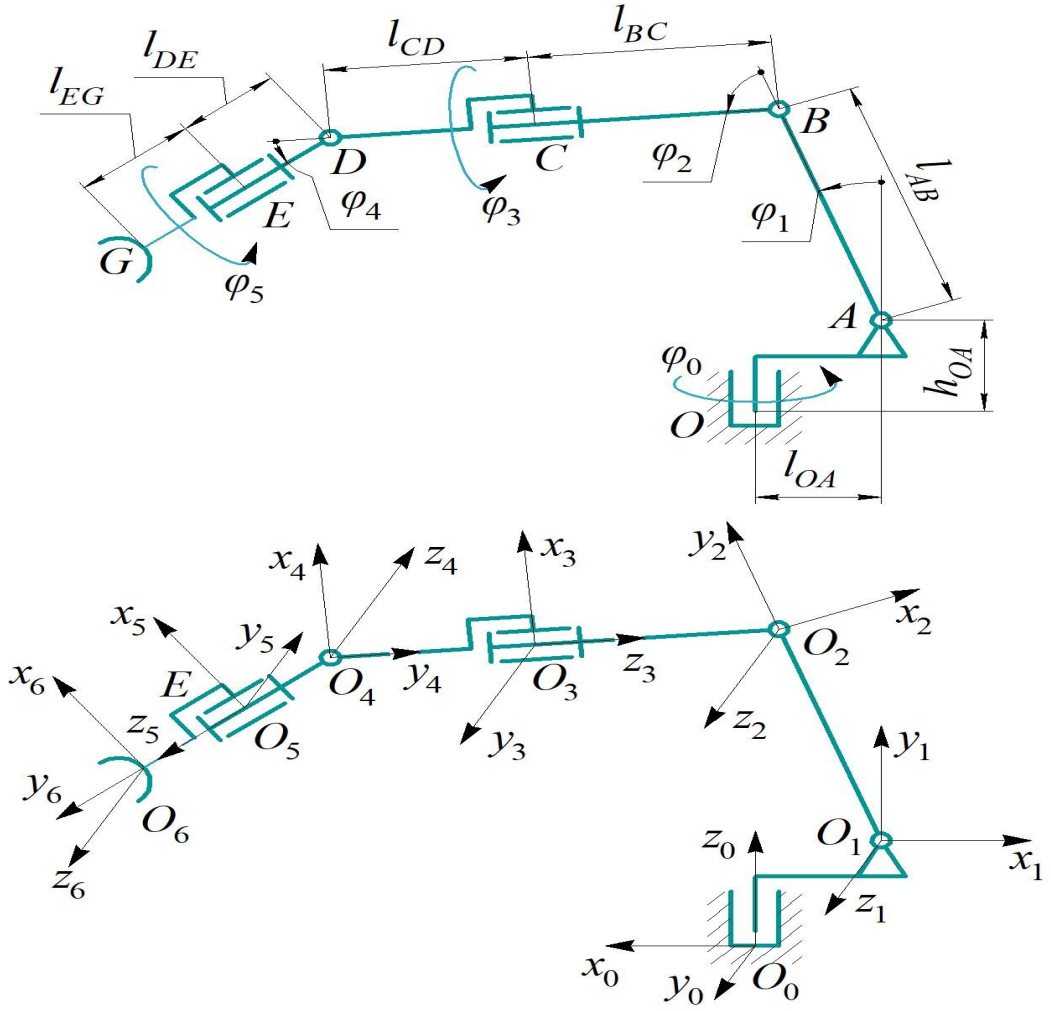

Figure 2: Kinematic schemes of the Telemax EVO Plus robot manipulator.

The kinematics of the Telemax EVO Plus manipulator are described using the Denavit–Hartenberg (DH) convention. [8] A base coordinate frame $O_0X_0Y_0Z_0$ is introduced such that O_0Z_0 is directed vertically upward along the turret rotation axis, O_0X_0 is directed forward in the look direction of the manipulator at the zero configuration, and O_0Y_0 completes a right-handed frame. For each link i, a local frame $O_iX_iY_iZ_i$ is assigned following the DH rules.

The generalized coordinates are $q=[\varphi_0,\dots,\varphi_5]^T$. The homogeneous transform between adjacent frames is defined by the standard DH matrix ${}^{i}T_{i-1}(\theta_i,d_i,a_i,\alpha_i)$. The link-specific DH parameters used in this work are listed in Table 4.

Table 4
DH parameters of the Telemax EVO Plus manipulator (adopted model)

Link	θ_i	d_i	a_i	α_i
1 (turret)	$\varphi_0+180°$	h_{OA}	l_{OA}	+90°
2 (shoulder)	$\varphi_1+90°$	0	l_{AB}	0
3 (forearm, upper)	φ_2	0	l_{BC}	0

4 (forearm, lower)	0	0	l_{CD}	φ_3
5 (wrist)	φ_4	0	l_{DE}	+90°
6 (gripper)	0	0	l_{EG}	φ_5

Using the DH parameterization, the accumulated homogeneous transformations $T_{0,i}$ are computed for each link. The upper-left 3×3 block gives the orientation, and the fourth column gives the link-frame origin in the base frame. These kinematic quantities provide the basis for the Jacobian velocity model and the subsequent energy-based Lagrangian dynamics. The end-effector Cartesian position is then defined by

$$r_G(q)=\begin{bmatrix} x_G(q) \\ y_G(q) \\ z_G(q) \end{bmatrix}, \tag{1}$$

taken from the translation component of

$${}^0T_6={}^0T_1\,{}^1T_2\,{}^2T_3\,{}^3T_4\,{}^4T_5\,{}^5T_6. \tag{2}$$

To support the subsequent dynamic formulation, the kinematic model is extended with link centre-of-mass positions and Jacobians. It is noted that the coordinate φ_5 does not change the Cartesian position (x_G, y_G, z_G) and only affects the tool orientation about its own axis. For each link i, the centre-of-mass position is defined as

$$r_{C_i}(q)=p_{0_i}(q)+R_{0_i}(q)r_{C_i}^i, T_{0i}=\begin{bmatrix} R_{0i} & p_{0i} \\ 0^T & 1 \end{bmatrix}, \tag{3}$$

where $r_{C_i}^{(i)}$ is constant in the local link frame. The linear and angular velocities of each centre of mass are expressed via Jacobians

$$V_{C_i}=J_i^v(q)\dot{q}, \omega_i=J_i^\omega(q)\dot{q}, \tag{4}$$

with Jacobian columns for revolute joints computed in the base frame as

$$J_i^\omega(:,j)=z_{j-1}, J_i^v(:,j)=z_{j-1}\times(r_{C_i}-r_{0_{j-1}}), \tag{5}$$

where z_{j-1} is the unit vector of the j-th joint axis obtained from $R_{0,j-1}$.

3.2. Energy-Based Formulation

The dynamic analysis of the manipulator is formulated through the Lagrange equation of the 2nd kind for generalized coordinates $q=[\varphi_0,\ldots,\varphi_5]^T, \dot{q}, \ddot{q}$, where $\varphi_0,\ldots,\varphi_5$ correspond to the rotation of the turret, elevation of the shoulder, bending of the forearm, rotation of the forearm sections, pitch of the wrist, and rotation of the gripper, respectively, taking into account dissipative forces (friction) and possible external forces/moments at the end effector point G.

In the energy-based formulation, the system dynamics are derived from the Lagrangian, defined as

$$L(q,\dot{q})=T(q,\dot{q})-V(q), \tag{6}$$

where q_i are the generalized coordinates and $\dot{q}$ are the generalized velocities T is the kinetic energy and V is the gravitational potential energy.

The kinetic energy of the serial manipulator is expressed as

$$T=\frac{1}{2}\sum_{i=1}^{6}\left(m_i v_{c_i}^T v_{c_i}+\omega_i^T I_{C_i}^{(0)}\omega_i\right)+\frac{1}{2}\dot{q}^T J_m \dot{q}, \tag{7}$$

where $I_{C_i}^{(0)}=R_{0i}I_{C_i}^{(i)}R_{0i}^T$ is the link inertia tensor expressed in the base frame, and $J_m=diag(J_{m0},\ldots,J_{m5})$ denotes the reflected rotor inertias of the actuators if rotor inertia data are available.

The potential energy in the gravity field is

$$V=\sum_{i=1}^{6} m_i g\, z_{C_i(q)}+m_L g\, z_G(q), g=9.81\,m/s^2, \tag{8}$$

where m_L is the payload mass (tool/load), and $z_{C_i}(q)$ and $z_G(q)$ denote the heights of the link centres of mass and the end-effector, respectively, in the base frame.

Using the Euler–Lagrange equations, the dynamics are written in the standard matrix form is

$$M(q)\ddot{q}+C(q,\dot{q})\dot{q}+G(q)=\tau-\tau_f+J_G^T(q)w_{ext} \tag{9}$$

where τ is the actuator torque vector, τ_f is the joint friction torque vector, $w_{ext}=[F_{ext}\,M_{ext}]^T$ is the external wrench at the end-effector point G, and $J_G^T(q)$ is the spatial Jacobian.

Friction is modelled as

$$\tau_f=F_v\dot{q}+F_c sgn(\dot{q}), \tag{10}$$

and, in the absence of experimental data, the viscous approximation $\tau_f=F_v\dot{q}$ is adopted.

We use the full dynamic model (inertia, Coriolis/centrifugal, and gravity terms) and a reduced positioning–orientation decomposition to compute the required joint torques for given joint angle trajectories.

3.3. Numerical Evaluation of Joint Torques in Wolfram Mathematica

The Telemax EVO Plus manipulator is modelled as an open serial spatial mechanism with six actuated revolute joints, described by the generalized coordinates $q=[\varphi_0,\ldots,\varphi_5]^T$. The joint torque profiles are evaluated numerically in Wolfram Mathematica by substituting prescribed joint trajectories $q(t),\dot{q}(t),\ddot{q}(t)$.The parameters with the next adopted values for the numerical study define the link geometry: $h_{OA}=75\,mm$, $L_{AB}=330\,mm$, $L_{OA}=50\,mm$, $L_{BC}=165\,mm$, $L_{CD}=250\,mm$, $L_{DE}=65\,mm$, $L_{EG}=130\,mm$, yielding the reduced 2R lengths $L_1=L_{AB}=0.330\,m$ and $L_2=L_{BC}+L_{CD}+L_{DE}+L_{EG}=0.610\,m$.

The required actuator torques are computed from the dynamic model in the form

$$\tau(t)=M(q)\ddot{q}+C(q,\dot{q})\dot{q}+G(q)+\tau_f(\dot{q})-J^T(q)w_{ext}. \tag{11}$$

For engineering evaluation of peak loads, a reduced model is used in which the positioning joints $\varphi_0,\varphi_1,\varphi_2$ are treated as dominant, while the wrist joints $\varphi_3,\varphi_4,\varphi_5$ are approximated by

decoupled second-order relations. In the planar 2R approximation for φ_1, φ_2 the link inertias are taken as $I_1 = \frac{1}{12} m_1 L_1^2$ and $I_2 = \frac{1}{12} m_2 L_2^2$, and the payload mass m_L is applied at point G at the distance $r_L = L_2$. because open-source datasheets do not provide inertial parameters for Telemax EVO Plus links, a consistent parameter set (masses, inertias, and viscous friction coefficients) is adopted from the technical documentation of the Telemax EVO Plus robot. [20-22]

The motion scenario used for torque evaluation is specified by boundary values of the generalized coordinates, including $\varphi_0 : 0^o \rightarrow 180^o, \varphi_1 : 110^o \rightarrow 55^o, \varphi_3 = \varphi_4 = 0^o, \varphi_5 : 0^o \rightarrow 360^o$, with a smooth start/stop law. The implemented Wolfram Mathematica workflow generates the prescribed joint trajectories and their time derivatives $(\dot{q}, \ddot{q})$, evaluates the torque profiles $\tau_i(t)$ and produces the corresponding plots.

4. Results and Discussion

4.1. End-effector trajectory

Figure 3 shows the three-dimensional end-effector trajectory for the studied (most loaded) scenario. The trajectory forms a smooth arc-like curve and passes close to the outer boundary of the workspace, which is consistent with operation at a large reach (significant *X* and *Y*) and a noticeable change in height *Z*. Along the *Z*-axis, the trajectory is predominantly monotonic and increasing: the initial segment lies near the lower workspace boundary, after which the end effector rises to approximately $Z \approx 0.55 \ldots 0.60$ m and then continues moving within this height range.

The projection onto the *XY* plane corresponds to an envelope motion around the robot: the trajectory spans a wide range of *X* (approximately from −0.6 to +0.7…0.8 m) and a substantial range of *Y* (up to ≈0.8 m). The absence of breaks or corner-like segments (the curve remains smooth) is consistent with the use of a smooth law for the generalized coordinates without jumps in velocities or accelerations, which is critical for reducing impulsive torque peaks in the actuators.

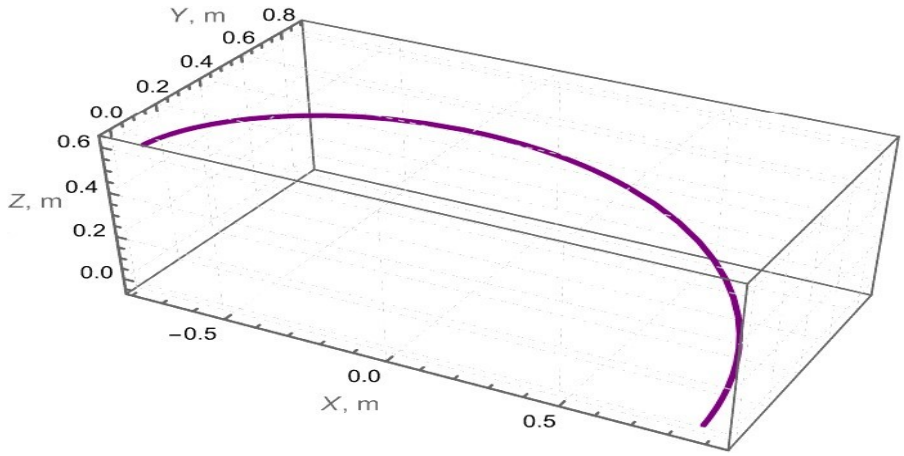

Figure 3: Investigated end-effector trajectory.

4.2. Torques in the base actuators

Figure 4 presents the modelled torques for the three base actuators: turret τ_0, shoulder τ_1, and forearm τ_2. The plots show that the shoulder actuator dominates, in terms of peak magnitudes, the following ordering holds $|\tau_1| > |\tau_0| > |\tau_2|$.

For the turret, τ_0 exhibits the following approximate peak values: a maximum of +30…31 Nm at $t \approx 0.20 \ldots 0.25$ s and a minimum of −24…−26 Nm at $t \approx 0.65 \ldots 0.70$ s, at the beginning and end of the motion $\tau_0 \rightarrow 0$. The sign change in τ_0 corresponds to the transition from acceleration (positive

torque) to braking (negative torque) under a symmetric velocity profile, and the zero crossing is interpreted as an indication that the turret load is predominantly inertial (acceleration/deceleration) rather than gravitational for the considered motion.

For the shoulder actuator τ_1, the largest magnitude occurs in the early phase: a minimum (largest magnitude) of −35…−36 Nm at t≈0.20…0.25 s. The smallest magnitude is observed around t≈0.80…0.85 s, where $\tau_1 \approx -14 \ldots -16\, Nm$. Notably, $\tau_1$remains negative at the beginning and end of the motion (approximately −25…−30 Nm at the start and −20…−25 Nm at the end), which is consistent with the dominance of the gravitational component. The reduction in $|\tau_1|$ around t≈0.80…0.85 s corresponds to a more favorable configuration.

For the forearm actuator τ_2, the reported approximate values are: a minimum of −16…−17 N·m at t≈0.20…0.25 s and a maximum (smallest magnitude) of −6…−7 Nm at t≈0.80…0.85 s. The overall curve shape is similar to τ_1, consistent with the fact that, in this scenario, the load is driven by the weight of the distal part (from the elbow to the gripper) and the associated inertial effects.

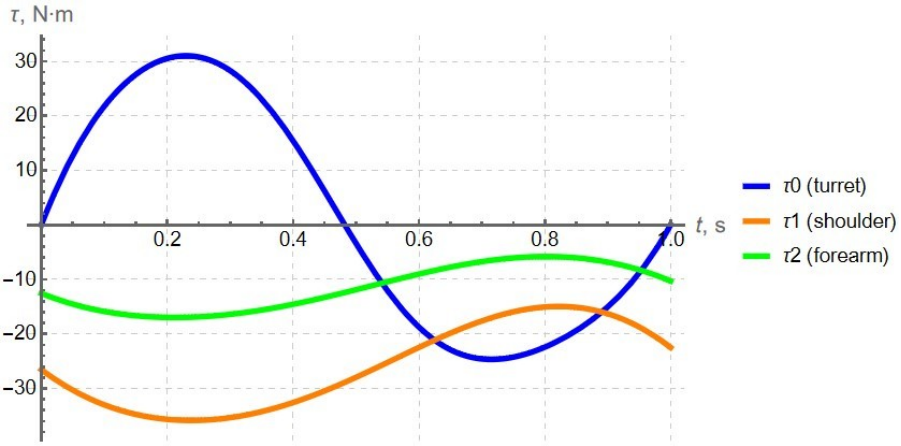

Figure 4: Modelled joint torque profiles for the manipulator (τ_0, τ_1, τ_2).

4.3. Torques in the wrist actuators τ_3, τ_4, τ_5

Figure 5 shows the torque profiles for the wrist actuators. The results indicate that τ_3 and τ_4 are practically zero throughout the entire interval. For the gripper rotation actuator, τ_5 reaches a maximum of approximately 0.34…0.36 Nm at t≈0.40…0.50 s; near the end, a small braking segment (a short negative interval) is observed, after which the torque returns to zero. The magnitude of τ_5 is two orders of magnitude lower than τ_0, τ_1, τ_2, indicating that, for the considered regime, rotation about the tool axis is kinematically active but energetically light.

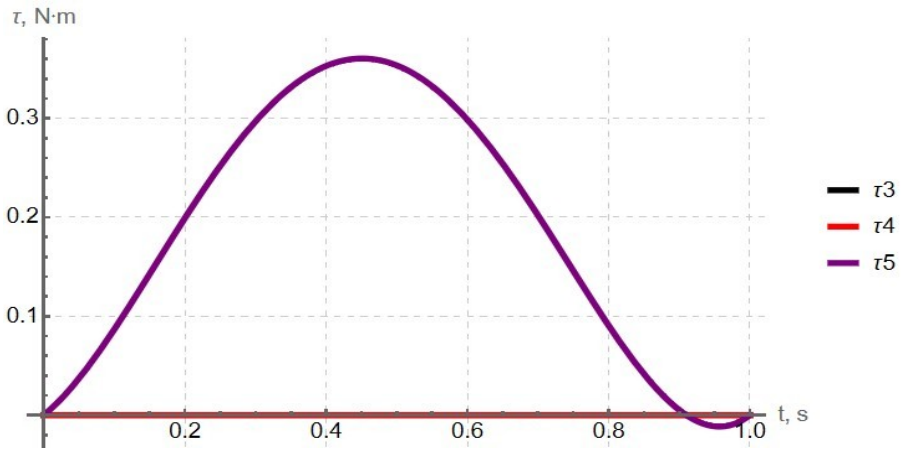

Figure 5: Modelled wrist joint torque profiles (τ_3, τ_4, τ_5).

5. Discussion

The results highlight a clear separation between positioning and wrist actuation in the investigated scenario. The torque demand is concentrated in the proximal drives, whereas the wrist torques remain negligible. This pattern is consistent with the adopted modelling decomposition into positioning and orientation, and with the stated kinematic property that φ_5 changes orientation without affecting (x_G, y_G, z_G). In practical terms, this supports the use of a reduced model for engineering load assessment, where actuator sizing and torque-limited planning are primarily driven by the positioning subsystem.

The turret torque profile differs qualitatively from the shoulder/forearm profiles. Its sign change and the tendency to approach zero at the start and end of the motion are consistent with an inertia-dominated load associated with acceleration and deceleration about the vertical axis, rather than a persistent gravity-driven component. In contrast, the shoulder and forearm torques retain a non-zero baseline level, which is compatible with a sustained gravitational contribution throughout the trajectory. The observed reduction in torque magnitudes towards the end of the motion coincides with the reported evolution of the end-effector height and workspace location, indicating that configuration-dependent gravitational leverage is a key factor shaping the proximal torque demand in this scenario.

The end-effector path is smooth and free of corner-like segments, which aligns with the use of a smooth law for the generalized coordinates. This is important because discontinuities in velocity or acceleration would manifest as impulsive torque peaks; the reported absence of such geometric irregularities provides an internal consistency check between the trajectory definition and the obtained torque profiles.

From an application standpoint, the presented case serves as a model-based example of predictive actuator-load estimation under a prescribed mission-relevant motion. Within the scope of the provided materials, the model output can be used to identify which joints constrain safe operation (here, the proximal drives) and to motivate the definition of admissible regimes that avoid unfavourable configurations associated with high gravitational loading.

The manufacturer inertial data are not available from open sources and that friction is treated using a simplified approximation in the absence of experimental data. Therefore, the reported torque levels should be interpreted as numerical estimates under the adopted parameter set and scenario, rather than as experimentally validated values.

6. Conclusion

The results highlight a clear separation between positioning and wrist actuation in the investigated scenario. The torque demand is concentrated in the proximal drives, whereas the wrist torques

remain negligible. This pattern is consistent with the adopted modelling decomposition into positioning and orientation, and with the stated kinematic property that φ_5 changes orientation without affecting (x_G, y_G, z_G). In practical terms, this supports the use of a reduced model for engineering load assessment, where actuator sizing and torque-limited planning are primarily driven by the positioning subsystem.

Declaration on Generative AI

During the preparation of this work, the authors used AI for grammar and language polishing.

References

[1] B. Siciliano, O. Khatib (Eds.), Springer Handbook of Robotics, Springer, 2016.

[2] B. Donald, P. Xavier, J. Canny, J. Reif, Kinodynamic motion planning, Journal of the ACM 40 (1993) 1048–1066. doi:10.1145/174147.174150.

[3] M.W. Spong, S. Hutchinson, M. Vidyasagar, Robot Modeling and Control, 2nd ed., Wiley, 2020.

[4] R. Featherstone, Rigid Body Dynamics Algorithms, Springer, 2007.

[5] K.M. Lynch, F.C. Park, Modern Robotics: Mechanics, Planning, and Control, Cambridge University Press, 2017.

[6] O. Khatib, Mobile manipulation: The robotic assistant, Robotics and Autonomous Systems 26(2–3) (1999) 175–183. doi:10.1016/S0921-8890(98)00067-0.

[7] B. Siciliano, L. Sciavicco, G. Villani, G. Oriolo, Robotics: Modelling, Planning and Control, Springer, 2009.

[8] J. Denavit, R.S. Hartenberg, A kinematic notation for lower-pair mechanisms based on matrices, Journal of Applied Mechanics 22 (1955) 215–221.

[9] R.P. Paul, Robot Manipulators: Mathematics, Programming, and Control, MIT Press, 1981.

[10] J.Y.S. Luh, M.W. Walker, R.P. Paul, On-line computational scheme for mechanical manipulators, Journal of Dynamic Systems, Measurement, and Control 102 (1980) 69–76.

[11] J.M. Hollerbach, A recursive Lagrangian formulation of manipulator dynamics, IEEE Transactions on Systems, Man, and Cybernetics 10 (1980) 730–736.

[12] J.J. Craig, Introduction to Robotics: Mechanics and Control, 4th ed., Pearson, 2017.

[13] Y. Umetani et al., Workspace and manipulability analysis of space manipulators, IEEE Transactions on Robotics and Automation 5 (1989) 86–99.

[14] J.F. Marques et al., Kinematics analysis of 6-DoF articulated robot with spherical wrist, Robotics and Autonomous Systems, 142 (2021) 103823.

[15] V. Sharma et al., Considerations on the kinematics analysis of an EOD robot's manipulator, in: Proc. IEEE ICRA, 2022.

[16] F. Karim et al., Sliding mode control design for EOD robot manipulator, Int. J. Adv. Manuf. Technol. 128 (2023) 2315–2328.

[17] M. Gutierrez et al., Analysis and evaluation of an EOD robot prototype, IEEE Access 10 (2022) 42895–42910.

[18] Ó. Hernández-Ortiz et al., Force control of bilateral teleoperated manipulators, Control Engineering Practice 104 (2020) 104609.

[19] A. Haddadi and K. Hashtrudi-Zaad, Bounded-Impedance Absolute Stability of Bilateral Teleoperation Control Systems, in IEEE Transactions on Haptics, vol. 3, no. 1, pp. 15-27, Jan.-March 2010, doi: 10.1109/TOH.2009.48.

[20] AeroVironment Inc., Telemax EVO Plus Datasheet, 2025. URL: *https://www.avinc.com/images/uploads/product_docs/2025_TelemaxEVOPlus_Datasheet_250717_v03.pdf* (accessed Dec. 1, 2025).

[21] Telerob GmbH, Telemax EVO Plus Technical Specifications, 2021. URL: *https://www.avinc.com/ugv/telemax-evo* (accessed Dec. 1, 2025).

[22] Altoy Defense Industry, Telemax EVO Plus Product Documentation, URL: *https://altoy.com.tr/telemax_en.html* (accessed Dec. 1, 2025).
[23] S. Guo et al., Tip-over stability analysis for a wheeled mobile manipulator, ASME JDSMC 139(5) (2017) 054501. doi:10.1115/1.4035234.
[24] A. Mazumdar et al., Improving robotic actuator torque density and efficiency, ASME DSCC, 2016. doi:10.1115/DSCC2016-9738.